Eco-Engineered Polyaniline-Fe_3O_4@Biochar Hybrid from Delonix regia Seeds for Dye Wastewater Purification

Gopalakrishnan Sarojini
grsarojini@gmail.com

Dhaanish Ahmed Institute of Technology

Perumal Murugan
Agni College of Engineering

Pownsamy Kannan
V.S.B College of Engineering Technical Campus

Research Article

Keywords: Polyaniline, Biochar, Congo red, Delonix Regia, Isotherm, Kinetics

Posted Date: August 1st, 2025

DOI: https://doi.org/10.21203/rs.3.rs-7259141/v1

Additional Declarations: No competing interests reported.

Eco-Engineered Polyaniline-Fe_3O_4@Biochar Hybrid from Delonix regia Seeds for Dye Wastewater Purification"

Gopalakrishnan Sarojini[a*], Perumal Murugan[b], Pownsamy Kannan[c],

[a] *Department of Food Technology, Dhaanish Ahmed Institute of Technology, Coimbatore, India*

[b] *Department of Chemical Engineering, Agni College of Engineering, Chennai, India*

[c] *Department of Chemistry, V.S.B College of Engineering Technical Campus, Coimbatore, India*

Corresponding author mail: grsarojini@gmail.com

Abstract

The current report examined the potential of polyaniline modified Fe_3O_4-Delonix regia seed biochar nanocomposite to adsorb congo red from synthetic wastewater. In this study, biochar was synthesized through carbonization process at a peak temperature of 500°C. Fe_3O_4 nanoparticles were synthesized using aqueous extract of Delonix regia seed pod. The consequence of pH, concentration and stirring speed on removal of congo red is examined. A maximum removal efficiency of 91.63% was obtained at optimal conditions of pH - 8, initial CR concentration – 50 mg/L and agitation speed - 500 rpm. The adsorption result demonstrated that experimental consequences fit well with Langmuir adsorption isotherm and pseudo second order kinetics was followed. A maximum sorption ability of 384.615 mg/g was obtained. Thermodynamic results shown that the sorption is spontaneous, reversible and endothermic one. The adsorption mechanism was explored and electrostatic attraction is the major rate controlling one. The current study established the efficiency of polyaniline modified Fe_3O_4-Delonix regia

seed biochar nanocomposite as an sorbent in removal of congo red. The solid agro waste is effectively transformed and applied in industrial wastewater treatment.

Key Words: **Polyaniline, Biochar, Congo red, *Delonix Regia,* Isotherm, Kinetics**

Introduction

In this modern era, industrial effluent roots for most of the health and environmental issues to water bodies and human. Most of the effluents from various sectors including plastics, rubber, polymer, printing, food, pharmaceutical and textile possess enormous amount of noxious synthetic dyes which are toxic to all lining creatures (Islam *et al*. 2019). Literature reports that about 280,000 tons of unprocessed dyes gets mixed with aquatic system globally (Talha Md *et al*. 2018). Among total synthetic dye consumption, 60% of azo dyes are most commonly employed in several industrial application (Sonwani *et al*. 2020). Azo dyes apart from being mutagenic and carcinogenic, has an ability to prevent the diffusion of sunlight into aqueous system which in turn affects the process of photosynthesis (Vikrant *et al*. 2018). Dye molecules cannot be degraded easily and persists in water bodies for prolong period of time causing severe health issues such as vomiting, diarrhea, nausea, etc. This impact trapped the attention of scientists and researchers to select appropriate method to remove dyes from dye laden waste water. Various technology including membrane filtration, coagulation, ion-exchange, biological oxidation, precipitation, photo chemical oxidation and adsorption are commonly employed to treat synthetic (Sarojini *et al*. 2021). All the above said techniques incur large amount of chemicals and expensive equipment (Reghioua *et al*. 2021). Also, the operational cost is high and it is difficult to obtain complete removal (Zhang *et al*. 2021). Rewards of adsorption process including simple in design, easy operation, low operating cost, high removal efficiency, ability to regenerate cum reuse promotes it as a high performance and effective technique in removal of dyes from wastewater. Many scientists are focusing to optimize the adsorption process and searching for new adsorbents with maximum sorption capacity with huge surface area and less cost. Most of them have succeeded in transformation of agro waste into better adsorbent. This attempt apart from reducing the environmental pollution also aims to recover and reuse waste resources.

Carbon biomass was prepared from various waste resources such as rice husk, tree residues, crop straw (Park *et al*. 2019). Biomass of carbon shows higher adsorption capacity, more surface activity and larger porous structure. Thermal stability, pore volume, specific surface area and surface hydrophobicity features have fascinated the attention of many researchers in wastewater remediation. Normally biochar, a porous carbon substrate is synthesized via biomass of different substances through pyrolysis process at high temperature (Kumar *et al*. 2021). It is an eco friendly feasible material for removing organic toxins from water bodies (Amen *et al*. 2020). Being a renewable source with low price and easy accessibility, biochar is highly recommended as sorbent in environmental remediation (Shaheen *et al*. 2022). Existence of functional clusters namely alkyl, carboxyl and hydroxyl groups enhance the biochar's adsorption capacity (Lian *et al*. 2019). Ability to create reactive oxygen radical via activation of peroxides makes it to find more application in wastewater remediation (Zhang *et al*. 2023). Porosity accounts for increased attention in removal of various pollutants (Shakoor *et al*. 2019). Many scientific reports confirmed the remarkable adsorption ability of biochar towards organic and inorganic pollutants (Tran *et al*. 2015). Carboneous resources including wood and coal are used to prepare commercial biochar and raw materials are expensive (Zhu *et al*., 2021). Agro wastes including seeds, fruit and nut shells are utilized to prepare low cost biochar through thermo-chemical process (Li et al. 2020).

More investigation work have been done out to improve biochar's adsorptive capacity. It has been recommended to use biochar powder instead of large sized biochar particles to obtain higher surface area (Tang *et al*. 2015). Fabrication of biochar composites have been suggested to obtain more active sites. Many studies reported that surface modification of biochar exhibited enhanced adsorptive ability (Zhang *et al*. 2018). In actual practice, large amount of uncoated biochar is required for detoxification of contaminants. Also, separation of pollutant loaded biochar is tedious. In the current scenario, conducting polymers owing to higher surface-area, chemical properties cum higher reactivity have gained increased attraction in elimination of toxins from water bodies.

Polyaniline is the furthermost preferred conducting polymers. It possesses unique properties namely excellent electrochemical activity, greater conductivity, ease preparation and bio-compatibility. Currently the application of polyaniline in waste water remediation has been enlarged in form of its composites and blends with metal oxides. Iron oxide nanoparticles have acquired enormous popularity in wastewater remediation due to its magnetic, biocompatibility and catalytic properties (Sarojini *et al*. 2023).

The iron oxide nanoparticles find its application in various sectors including drugs vector, magnetic resonance imaging contrast agents, adsorption of antibiotics, heavy metals and dyes (Zheng *et al*. 2023). Inspite of all advantages, iron oxide nanoparticles tens to agglomerate and biosynthesis involves low yield of nanoparticles (Mondal *et al*. 2020). Biochar based hybrid nanocomposites has the potential to overcome these restraints. Biochar based nanocomposites shows higher yield production. The iron oxide nanoparticles and polyaniline are coated on the surface of biochar and utilized for potential purpose (Sharma *et al*. 2022).

In this research, biochar was obtained from seed pods of Delonix Regia and to improve physiochemical characterics, enhance recovery and increase removal efficiency, the synthesized biochar was impregnated with iron oxide nanoparticles. The incorporation of iron oxide nanoparticles on the biochar's surface increases the quantity of available active sites (Yu *et al*. 2022). Smaller magnitude, higher surface area and improved adsorptive activity enhances the removal efficiency of biochar nanocomposite. Active functional groups available on the surface reduce the agglomeration of nanoparticles (Hossain *et al*. 2022). Generally, Biochar natured nanocomposite retains the parental belongings of biochar as well as nanoparticles to remove pollutants from wastewater. Magnetic nanoparticles enable easier magnetic separation of biochar nanocomposites. However only few reports are available on magnetic incorporation and surface modification of biochar.

The present work focused on the preparation of biochar hybrid nanocomposite from Delonix Regia and iron oxide nanoparticles from Delonix Regia seed pod. To enhance its adsorptive efficiency, the synthesized biochar was incorporated with iron oxide nanoparticles and polyaniline. The synthesized polyaniline-iron oxide biochar nanocomposite was characterized by Fourier Transform Infra-Red Spectroscopy (FTIR), Scanning Electron microscope (SEM), EDX and X-Ray diffraction (XRD) and its physiological properties were analyzed. The optimum value and consequence of process parameters were investigated. The reusability studies of the nanocomposite was also examined. The mechanistic approaches involved in adsorption removal of congo red was discussed.

Materials and methods

2.1 Materials

Ferric chloride, ferrous chloride, aniline, perammonium sulphate, acetone were purchased from Sisco research laboratories, Mumbai.

2.2 Preparation of aqueous extract

Delonix regia seed pods was collected from Coimbatore. The specimen was dried and grounded. 5 g of dried sample is mixed with 50 mL of water and the mixture is heated at 100˚ C for 15 min. The filtrate is used for the preparation of iron oxide nanoparticles.

2.2 Biosynthesis of Fe_3O_4 nanoparticles

Fe_3O_4 nanoparticles were synthesized using 1:2 molar ratio of ferric chloride and ferrous chloride mixture (Kataria *et al*. 2018) The aqueous extract of Delonix regia seed pods was used as a reducing agent. To appropriate amount of Delonix regia aqueous extract, the iron solution mixture was added and the solution pH was adjusted to 11. The change of color from black brown to black specifies the development of iron oxide nanoparticles. The collected precipitates were dried in oven at 100˚ C.

2.3 *Synthesis of Delonix Regia biochar*

Seeds of Delonix Regia seeds were cleaned using de-ionized water to eliminate the dust and scums. After cleaning, seeds were oven-dried for 48 h at 60° C to eliminate bounded moisture. Further, the dried seeds were crushed in a grinding mill and sieved to obtain particle size of 6μm. Then they are pyrolyzed at 300°C for 3 h to yield biochar (Emenike *et al*. 2022).

2.4 Synthesis of polyaniline - Fe_3O_4-Delonix Regia biochar

The iron oxide nanoparticles and biochar was dissolved in 1.02g of aniline monomer dissolved in HCl solution (0.5 M solution of 50 ml in quantity). The solution was sonicated for 30 min and stirred continuously for 2 h using magnetic stirrer. About 0.2 g of ammonium persulfate was liquified in HCl solution (20 ml of 0.5 M). This is then mixed with the above solution in dropwise. The entire blend is kept in an ice bath for 4 h and stirred by means of a magnetic stirrer. The mixture was left to react for 24 h. The obtained blackish precipitate was filtered, washed, washed with deionized water and dried at 80°C in an oven (Zhou *et al*. 2019).

2.4 Characterization of polyaniline- Fe_3O_4-Delonix regia seed biochar nanocomposite

The synthesized biochar-based nanocomposite was analysed using X-ray diffractometer, Fourier transform infrared spectroscopy analysis (FTIR) (Thermo Nicolet, Avatar 370), SEM/EDX.

2.5 Adsorption of dye by Fe_3O_4- Delonix Regia seed biochar nanocomposite

To evaluate the adsorption performance of biochar nanocomposite about 0.01g of biochar nanocomposite powder was mixed with 50 ml of CR (initial concentration of 10 mgL^{-1} of varying pH). The solution was shaken in an orbital shaker for 1 h and the adsorption capacity at various pH was evaluated to chose optimum pH. Adsorption isotherm experiments were performed by adding 0.01 g of biochar nanocomposite to 50 ml of various ranges of CR initial concentration and shaken at different temperatures. CR dye concentration was examined in a double beam UV–Vis spectrometer at 232 nm. The removal efficiency and sorption ability was calculated by change in concentration of CR before and after adsorption by using the equation given below (Eqns (1) and (2))

$$\%R=\frac{(c_i-c_t)}{c_o}\times 100 \qquad (1)$$

$$q_e = \frac{V}{m} \times (C_i - C_e) \quad (2)$$

Where C_i - bulk concentration of congo red, C_t - final congo red concentration and C_e are equilibrium congo red concentration, and m - mass of biochar nanocomposite (mg).

2.6 Optimization Analysis

Experimentation for the sorptive removal of CR dye was performed using the Box-Behnken design (BBD). The parameters viz. pH (2–12), initial congo red concentration (10–90mg/L) and stirring speed (100-500 rpm) were optimized. The parameter levels were given in Table 1.

2.7 Regeneration of Fe_3O_4- Delonix regia seed biochar nanocomposite

Polyaniline modified Fe_3O_4- Delonix regia seed biochar nanocomposite was regenerated by 0.1 M NaOH solution. The CR sorbed biochar nanocomposite was reactivated using 0.1 M HCl solution. About 0.01 g regenerated biochar nanocomposite was added to 25 mL of 50 mg/L of CR solution. The solution was shaken for at 30°C for 4 h. It was regenerated and further reused for 4 consequent cycles.

3. Results and Discussions

3.1 Interpretation of biochar nanocomposite

3.1.1 FTIR Spectral analysis

Fig 1 (a) depicts the spectra of biochar nanocomposite. The broad band in the narrow range of 700 cm^{-1} attributes to Fe-O stretching of metal oxides (Thomas et al. 2020). Several adsorption bands attributing to various functional groups are noticed in FTIR spectral image of biochar nanocomposite before adsorption. The broad vibration band visible in the range of 3379 cm^{-1}

attributing to O-H group stretching vibration suggests the existence of hydroxyl group on the nanocomposite's (Jiang et al. 2023). This might have raised by hydrogen bonding linkage with lignin, cellulose and pectin. The peak at 2923 cm^{-1} links to C-H stretching of alkyl group. The emerging peaks at 1989 cm^{-1} stands for C=O stretching vibration of ester, ketone and aldehyde groups which are components of hemicellulose. The crew at 2322 cm^{-1} attributes to C-O aliphatic groups. Visible band at 1578 cm^{-1} match to N-H or N-O asymmetric stretching vibration (Mao *et al*. 2022).

A representative peak at 1472 cm^{-1} attributes to C-C stretching vibration revealing the presence of aromatic species. A weak intensity peak at 1074 cm^{-1} allotted to C-O stretching vibration suggests the presence of acidic groups. The representative peaks in the range of 875 cm^{-1} attributes to C-H aromatic vibration (Dai *et al*. 2018). Theses vibrational bands reveals that biochar contains lignin, fatty acid and cellulose. A band at 3379 cm^{-1} attributes to the N-H stretching. A distinguishing peak at 1578 cm^{-1} is allotted to the stretching vibration of quinone and benzene rings. The peak at 1297 cm^{-1} links to the C-N stretching vibration (Zhou *et al*. 2016). These are characteristic peaks of polyaniline which evidence the presence of polyaniline in hybrid composite.

Fig 1b represents the FTIR field of biochar nanocomposite after congo red adsorption. After congo red adsorption, the FTIR spectrum gets changed. The existence of new points at 1926 cm^{-1} witnesses the adsorption of congo red dye. The peak at 1926 cm^{-1} is the characteristic absorption peak of congo red (Awang *et al*. 2017). Formation of new chemical bonds signifies the existence of sorption process. The observed changes in characteristic bands after adsorption implies the participation of corresponding functional clusters in the elimination of CR (Rai *et al*. 2018). Modification in strong peak of 3455 cm^{-1} signifies the contribution of hydroxyl group in adsorption of congo red and involvement of hydrogen bonding mechanism (Jiang *et al*. 2023). Most of the researches report that carboxyl, hydroxyl and phenolic group are reasonable for adsorption of dye via ion exchange process. Hence it could be expected that availability of lactonic, phenolic, hydroxyl and carboxylic groups in biochar would result in improved sorption capacity (Emenike *et al*. 2022).

3.1.2 Surface Analysis of synthesized nanoparticle

Biochar nanocomposite's removal effectiveness highly depends on the surface sound structure. SEM image of biochar nanocomposite is showed in Fig. 2. It was detected that surface was heterogeneous and irregular. SEM image confirms the non-uniform porosity. Sufficient amount of pores and cavities were found on the surface. The pores are in different size and shape. At higher temperature lignocellulosic substances to tend to degrade whereby volatile substances escapes forming mesopores and micropores (Ahmad *et al*. 2015). Similar type of images are obtained in nanocomposite of nano valent silver doped biochar obtained from algae (Shaikh *et al*. 2022). Pores of various sizes are formed to due to higher activation temperature. The image also confirms the effective coating of Fe_3O_4 nanoparticles on biochar's surface. Presence of larger proportion of iron precursor causes to agglomerate. SEM image also displays the attachment of polyaniline particles on the composite. From BET analysis, the surface area of biochar and biochar nanocomposite was found to be 25.63 m^2/g and 245.89 m^2/g respectively. Hence, surface area of biochar nanocomposite got increased due to attachment of iron -oxide and polyaniline particles (Sun *et al*. 2012). SEM image of after adsorption has clearly picturized that adsorption has occurred and white particles visible on the surface are due to the attachment of CR dye on the surface. Micropores present on the surface disappeared due to the occupation of vacant sites by congo red dye molecule.

3.1.3 Surface charge

Surface charge of biochar nanocomposite was determined by evaluating point of zero charge (pH_{ZPC}). pH Drift method was employed to calculate pH_{ZPC}. Point of zero charge helps to propose the mechanism related with adsorption. pH_{ZPC} of biochar nanocomposite was found to be 6.8 whereas the pH_{ZPC} of biochar was 4.2 (Fig. 3). The pH_{ZPC} of biochar nanocomposite was found to be higher than pH_{ZPC} of biochar. Based on the outcomes it could be supposed that surface of biochar nanocomposite tends to remain +ve ly charged for pH less than 6.8 and for pH greater than 6.8 it is negatively charged.

3.1.4 XRD pattern

Fig. 4 displays the XRD diffraction pattern of biochar nanocomposite. Intense peaks at 2θ = 35.89 ° indicated the crystallinity nature of biochar nanocomposite. It corresponds to parallel and perpendicular periodicity of polyaniline chains. The reflection peaks of biochar also reflects the crystallinity nature which might attributed to presence of hemicellulose, cellulose along with lignin. The peaks observed confirms the successful doping of Fe_3O_4 nanoparticles and shows that propertie sand crystallinity nature of Fe_3O_4 nanoparticles remains unaltered even after impregnation. Similar diffraction pattern was obtained in the characterization of CIP@Fe_3O_4@PANI composites (Chen *et al*. 2021)

3.3. BBD based optimization and statistical analysis

The CR removal, both experimental and projected, are provided in Table 2. Best model is obtained using quadratic model, with high R^2 value and it is given below:

$$\text{CR removal} = -57.68341 + 11.08312\,\text{pH} + 1.66891\,\text{CR IC} + 0.272949\,\text{AS} - 0.005487\,\text{pH} * \text{CR IC} + 0.000548\,\text{pH} * \text{AS} - 0.000425\,\text{CR IC} * \text{AS} - 0.702\,\text{pH}^2 - 0.01353\,\text{CR IC}^2 - 0.000203\,\text{AS}^2$$

ANOVA (Analysis of variance) is employed to analyze CR sorption process (Table 3). A low p value of lack of fit (0.0001), high F value (1645.8), high R^2 (0.9995) demonstrates the fitness of BBD modeling. The effects pH, congo red initial concentration (CR IC), agitation speed (AS) had positive effects on congo red adsorption. The linear, interactive and square effects of all the three variables are found to be significant. The 3D plots validated that the interaction among the chosen parameters were difficult to understand and nonlinear.

3.3.1 Outcomes of pH

The consequence of pH and initial CR concentration on CR sorption using the synthesized biochar nanocomposite was depicted in Fig. 5. Under pH array 2–12, the CR elimination increased as pH is increased from 4 to 8 while after that CR elimination decreases slowly. This is because, from the zeta potential concept, high concentration of OH-ions makes the surface charge of biochar nanocomposite -ve^{ly} charged for above pH 6.8 which unfavours CR adsorption. However, below pH 7, high concentration H+ ions turn the biochar surface to +ve^{ly} charged which accounts for sorption of negatively charged CR dye molecule. This led to strong electrostatic interactions between biochar and congo red and increased the electron-acceptability of congo red which in turn increased the sorption ability at lower conditions. An electrostatic repulsion exist among nanocomposite and suphonate ions of congo red dye molecule under basic pH. The positive sign of the coefficient of the parameters designates that an increase in the parameters produces a rise in the CR removal efficiency (Sarojini *et al*. 2021b). This is evident from the modeling equation and ANOVA.

3.3.2 Outcomes of CR initial concentration (CR IC)

The interactive effect of CR IC with pH and AS is depicted in Fig. 6 and 7 respectively. From these figures it is inferred that the CR removal increases as initial concentration of CR increases from 10 to 55 mg/L. But further increase in CR IC causes a reduction in CR removal. Even though high CR IC helps in higher diffusion, the actives sites of biochar were inaccessible at higher CR IC. This results in low sorption percentage of CR. This is also well supported by many literatures (Agilandeswari *et al*. 2024a)

3.3.2 Outcomes of Agitation Speed (AS):

Interaction effects of AS with pH is presented in Fig. 6. CR removal increases with increase in AS from 100 to 500 rpm. It shows that, at this rpm, the sorbent are in suspension and the readiness of interaction active sites and more surface area produces an increased CR sorption onto biochar nanocomposite. The results are well supported by (Agilandeswari *et al*. 2024b)

3.4 Thermodynamic parameter Analysis

The impact of temperature on congo red removal was observed by varying the temperature among 298 K and 323 K. The outcomes are given in Fig. 8 and it was noted that temperature raise boosts up the removal efficiency of congo red and it remains maximum up to 303.15 K. At 303.15 K the molecules possess adequate energy to reach and react on the binding sites on biochar nanocomposite surface. Increase in temperature up to 323.15 K causes decrease in removal efficiency. It suggests that elevated temperature is not favoring for sorption of congo red by the synthesized composite.

Gibbs free energy ($\Delta G°$), $\Delta S°$ and $\Delta H°$ were calculated using the equation given below:

$$\Delta G^0 = -RT \ln k \qquad (5)$$

$$\Delta G^0 = \Delta H^0 - T\Delta S^0 \qquad (6)$$

Congo red adsorption onto hybrid biochar nanocomposite was confined using thermodynamic characteristics. The thermodynamic constants evaluated at various temperature are provided in Table 4. The -ve values of ΔG at various temperature indicated that sorption was spontaneous process. +ve of ΔH° proposed the endothermic nature of the sorption and +ve of ΔS° proposed enhanced randomness at the solid-solution interface (Jayakumar *et al*. 2021).

3.5. Adsorption analysis of isotherms

Various isotherm models were selected for examining the correlation of CR sorption equilibria data. The constants evaluated and statistical parameters are provided in Table 5 along with the isotherms employed. The isotherm with correlation coefficient value higher than 0.90 exactly fits the experimental data with predicted values. The CR sorption isotherm data are depicted in Fig. 9 and Table 5. Langmuir isotherm is proposed on the assumption that surface of adsorbent contains enormous active sites and each site possess uniform energies. It is observed that Langmuir model shows the best fitting degree (R^2=0.9954). The values of R_L fitted by Langmuir was smaller than 1 indicating that the adsorption conditions facilitate adsorption (Langmuir *et al*. 1918). Also the results conveys that the surface of biochar composite was regular and homogeneous. Value of 1/n of Freundlich parameters was between 0 and 1, which also evidenced that adsorption was preferential process (Freundlich *et al*. 1906). Temkin isotherm model also had a highest degree of correlation coefficient indicating the involvement of strong intermolecular forces in the adsorption (Temkin *et al*. 1940), D-R isotherm results showed that the value of E=0.7747 which is less than 8 suggesting the sorption to be physical in nature (Tan et al. 2015). From the above observations, it could be concluded that the Langmuir isotherm was followed.

3.6 Adsorption analysis of kinetics

Kinetics is very much essential in contaminant removal as it gives detailed information regarding rate, mechanism and rate determining steps. The kinetics of congo red dye adsorption onto biochar hybrid composite was explored using well-known pseudo I order (PFO), pseudo II order (PSO), intraparticle diffusion (IPD), Elovich and Power kinetic models. Various kinetics models employed to determine rate kinetics are provided in Table 6. The consequences of kinetic data are revealed in Tables 6 and plots are represented in Fig. 11. Pseudo II order model fit the kinetic data better than other models. The removal efficiency was found to be higher than 90%. Adsorption was found to be faster in earlier 10 minutes and slows down to reach adsorption equilibrium at around 90 minutes. The chemisorptive nature of congo red adsorption on biochar hybrid composite was confirmed by isotherm analysis. At low initial concentrations, the equilibrium concentration (Qe) values was minimum, then with increase in final concentration, the (Qe) values climbed. This is because of combined diffusion at higher concentrations.

3.7 Mechanism

Surface properties of biochar nanocomposite contributes a chief part in the sorption process (Tan et al. 2015). Heterogeneity surface and carbonization degree decides the maximum extent of adsorption. Pyrolysis temperature involved in biochar production also pays a major part in adsorption. Pyrolysis temperature of 500°C promotes the formation of carboneous material by converting organic materials into aromatic carbon and degradation of cellulose, hemicellulose and lignin of raw material takes place (Lee et al. 2018). Electrostatic interaction, partitioning, hydrogen bonding, π-π bonding hydrophobic interaction and pore filing are suggested adsorption mechanism. Solution pH and point of zero charge (pH_{zpc}) plays a major role in adsorption. Point of zero charge (pH_{zpc}) is directly connected with solution pH and it gives essential idea about surface charge of biochar nanocomposite. At higher pH, surface remains negative charged due to the presence of abundance –OH groups whereas surplus hydrogen ions makes the surface to stay positively charged at lower pH. However at pH lower than pH_{zpc} (6.8), positively charged biochar nanocomposite surface was favourable for adsorption of CR molecule. Electrostatic attraction among positive charged surface and negatively charged CR species accounts for adsorption of CR. Most of research studies conveyed that electrostatic attraction is dominant part in the sorption of organic pollutants on biochars (Ambaye *et al*. 2022). FTIR spectral images of after absorption of CR shows that adsorption occurs by means of hydrogen bonding also. The shift in peak of 1126 cm^{-1} witness that hydrogen bonding is accountable for CR adsorption. The peak of C==C was weakened after adsorption suggests that π-π interaction was also responsible for adsorption of CR.

3.5 Reusability property of polyaniline modified Fe_3O_4- Delonix regia seed biochar nanocomposite

In waste water remediation, the most important concern deals with feasibility and economical issue. The economy of process depends on reusability of adsorbent for many cycles without any loss in its efficiency. Also attention should be paid to disposal of pollutant adsorbed adsorbent. The adsorbed pollutant should be removed prior to its disposal. Otherwise it may create secondary pollution. Here the dye laded nanocomposite was reactivated again using 0.1M NaOH and reused for dye adsorption. The reactivated biochar nanocomposite also exhibited better adsorption performance. The adsorption capacity of biochar nanocomposite remains unchanged even after 4 consecutive adsorption /desorption cycles (Fig. 10). Table 7 indicated the adsorption capacity of various biochar in elimination of CR dye under optimal conditions. The results showed that biochar nanocomposite possess higher adsorption capacity than any other biochar based nanocomposites. Therefore it is witnessed that polyaniline modified Fe_3O_4- Delonix regia seed biochar nanocomposite can serve as an high efficient and reusable adsorbent.

4. Conclusion

Polyaniline hybrid biochar composite was prepared by in-situ oxidative polymerization of aniline monomer. The synthesized biochar composite was effectively employed to remove CR dye by sorption. Biochar enlarged the surface area and pore size whereas polyaniline polymer increased the adsorptive capacity through polaran, amine and imine groups. Electrostatic interaction, partitioning, hydrogen bonding, π-π bonding hydrophobic interaction and pore filing involved in the sorption of CR dye. The uptake of synthesized biochar was found to 384.615 mg/g and Langmuir isotherm was governing. PSO kinetics was found to be mechanism of CR sorption. The biochar composite possessed admirable desorption and it can be recovered using 0.1M NaOH. The biochar nanocomposite efficiency remains unchanged after 4 consecutive adsorption/desorption cycles. Thus, the composite can serve as an effective sorbent for removal of CR dye.

List of Figures

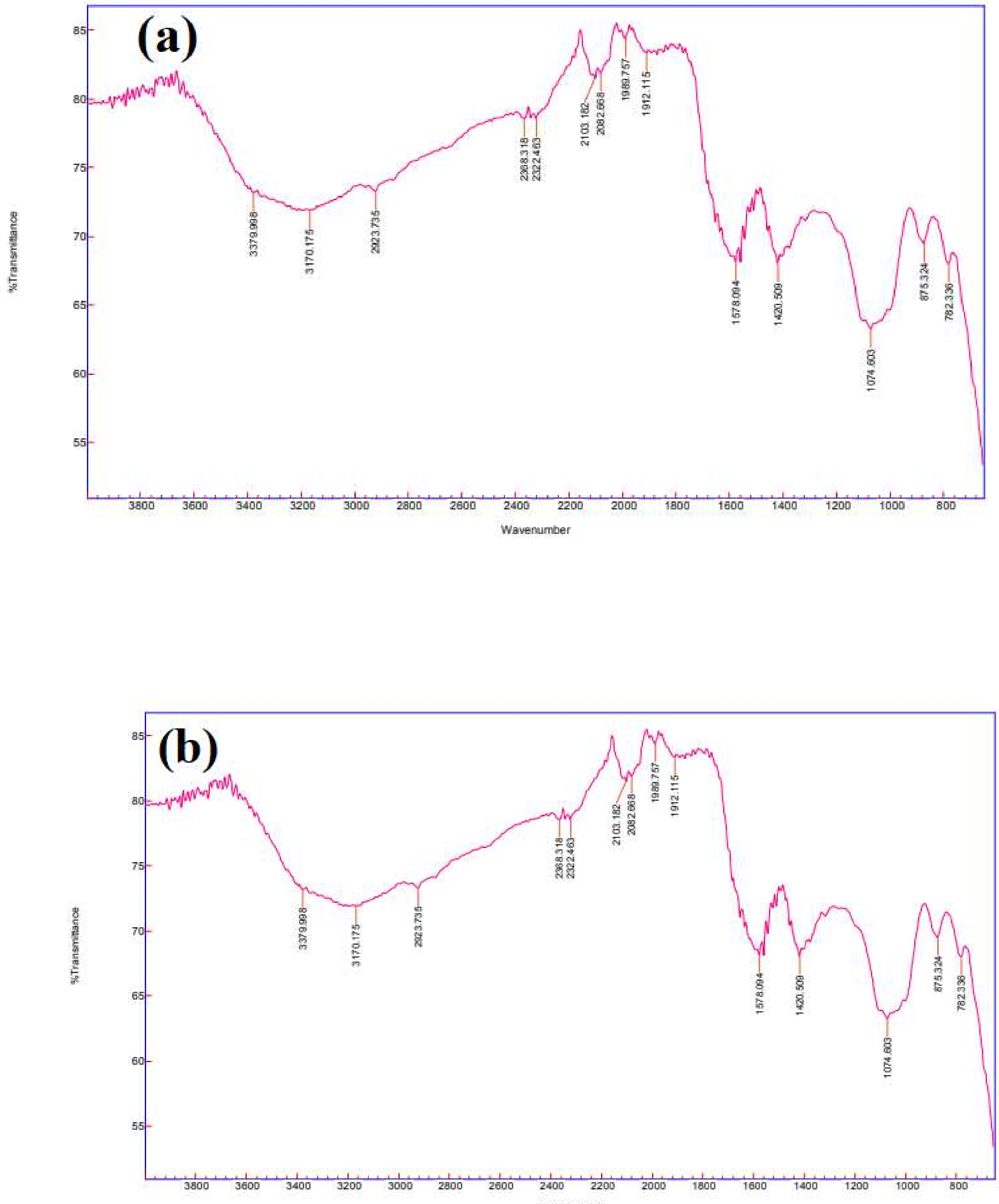

Fig. 1. FTIR of Biochar nanocomposite (a) before sorption of CR (b)after sorption of CR

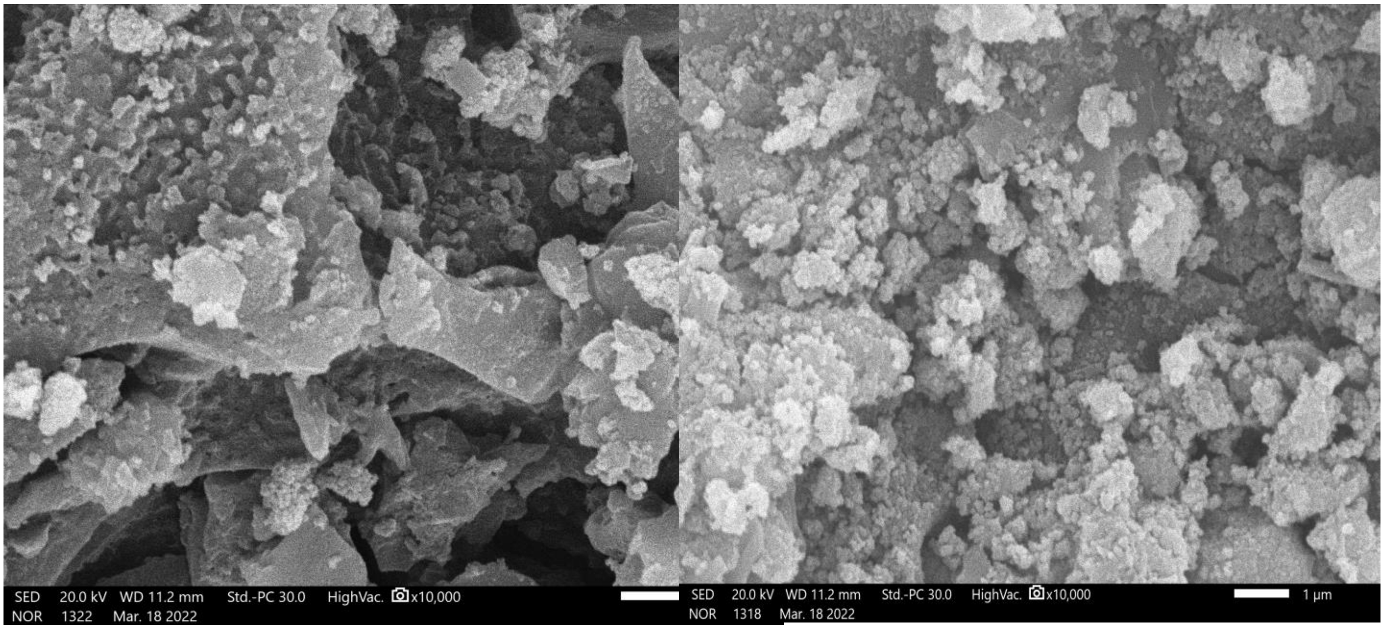

(a) **(b)**

Fig. 2 SEM for nanocomposite (a) before sorption and (b) after CR adsorption.

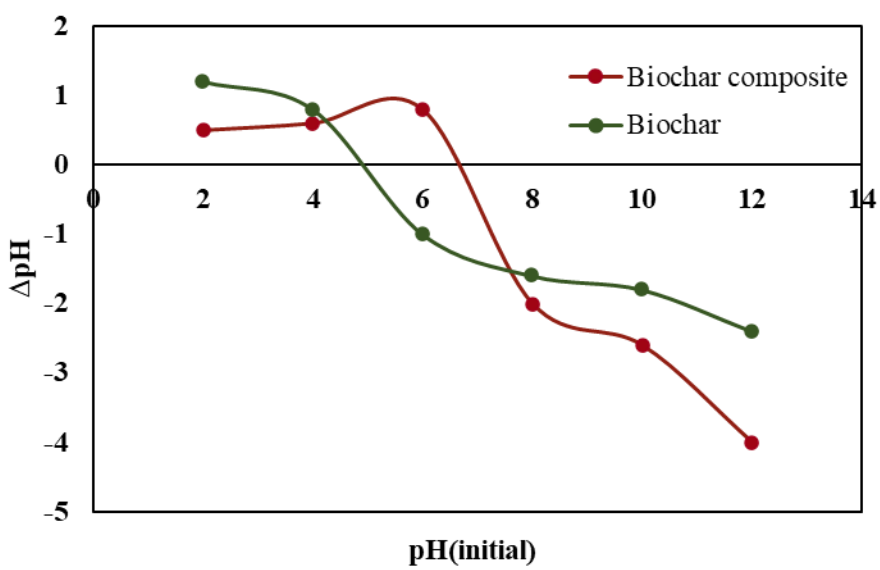

Fig.3. Zero-point charge measurement

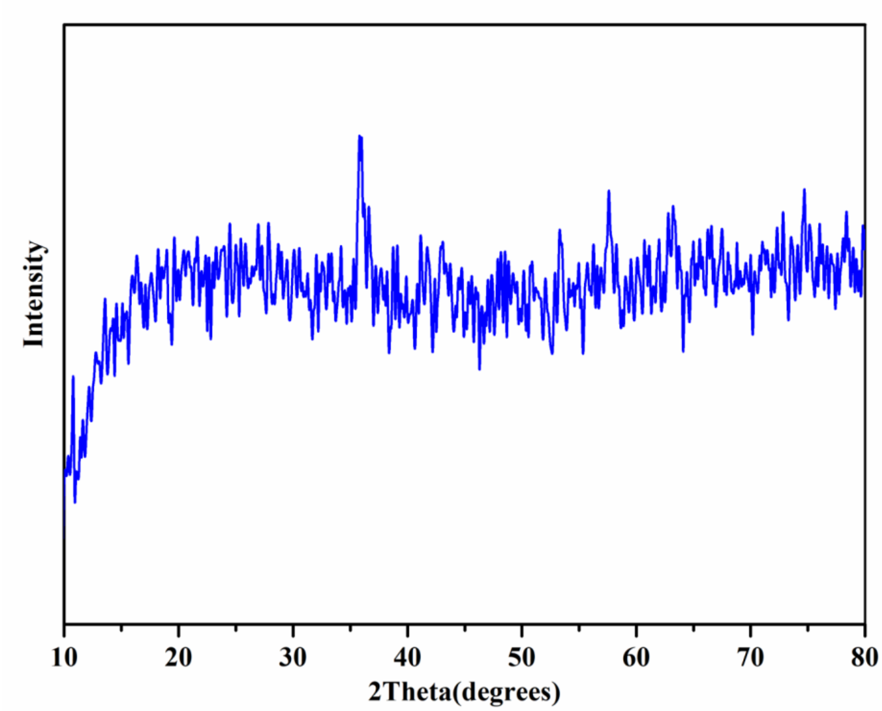

Fig. 4. XRD Spectrum of biochar composite

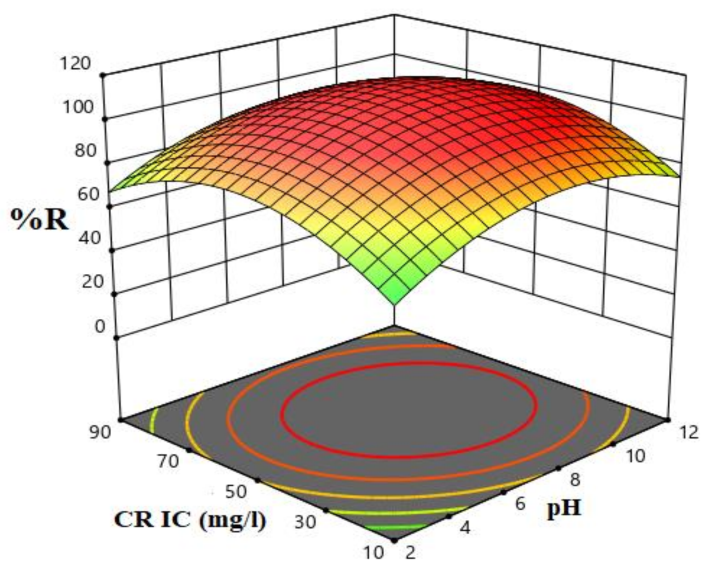

Fig. 5. Effect of pH and concentration on CR removal

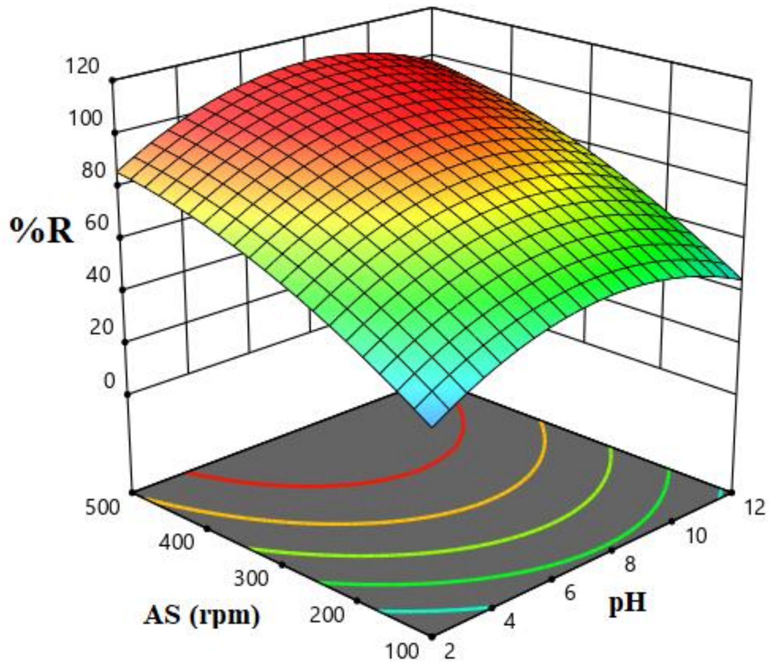

Fig. 6. Effect of pH and agitation speed on CR removal

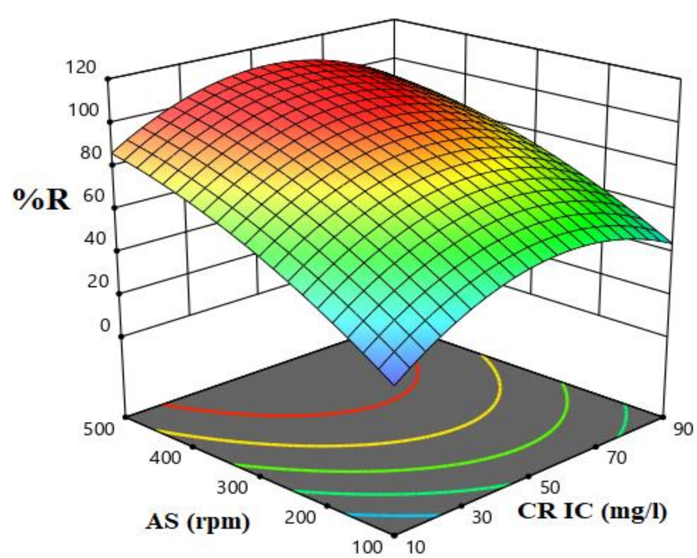

Fig. 7. Effect of concentration and agitation speed on CR removal

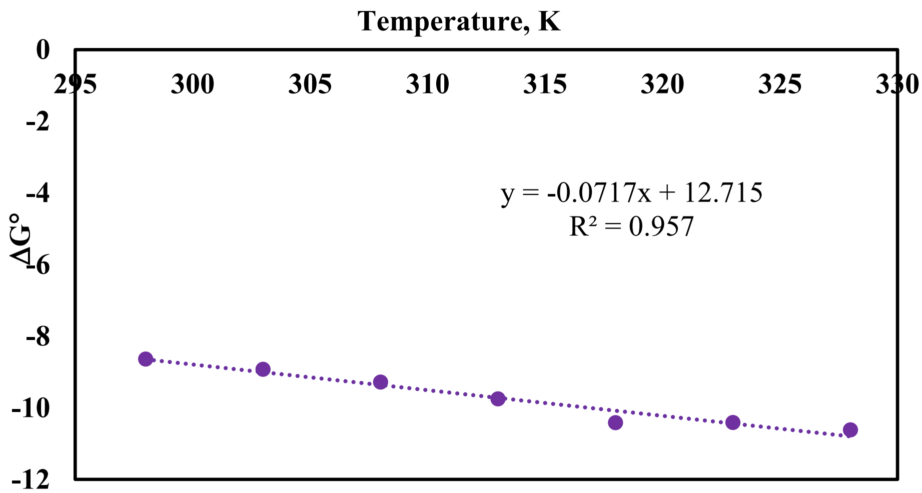

Fig. 8. Thermodynamic plot for the sorption of congo red

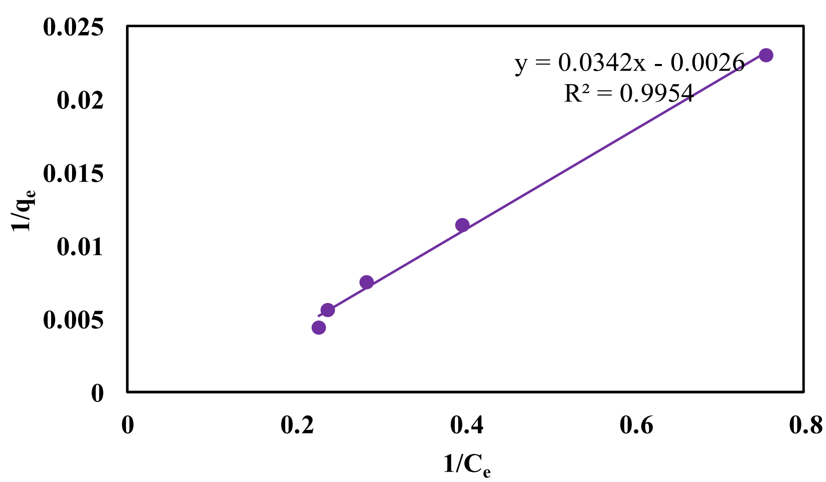

(i)

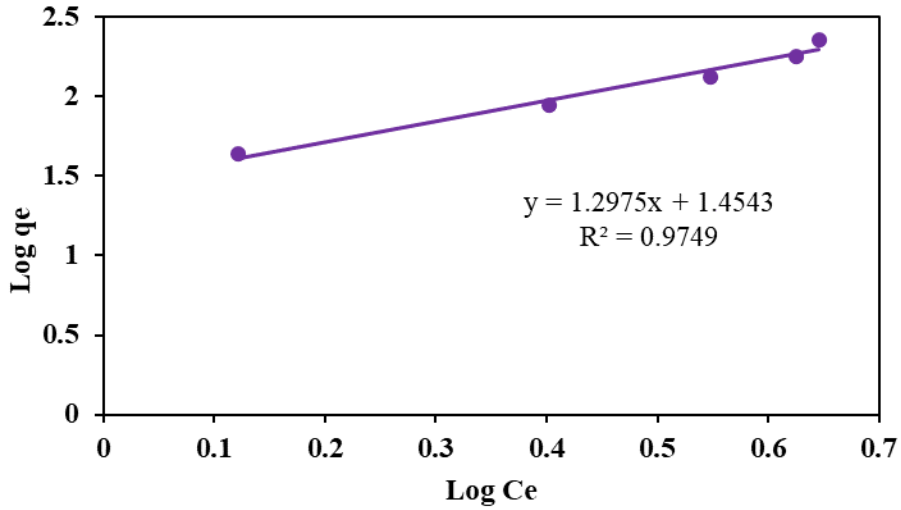
2.5
2
1.5
1
0.5
0
Log qe
y = 1.2975x + 1.4543
R² = 0.9749
0
0.1
0.2
0.3
0.4
0.5
0.6
0.7
Log Ce

(ii)

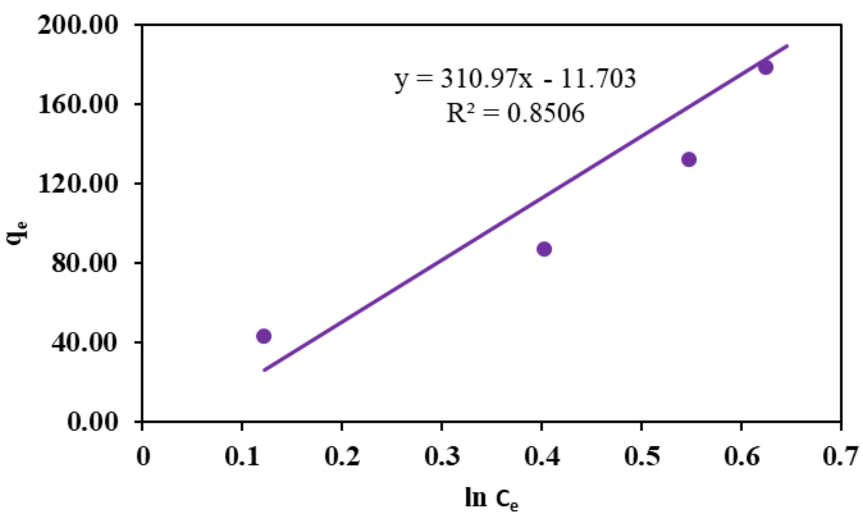
200.00
160.00
120.00
80.00
40.00
0.00
qe
y = 310.97x - 11.703
R² = 0.8506
0
0.1
0.2
0.3
0.4
0.5
0.6
0.7
ln ce

(iii)

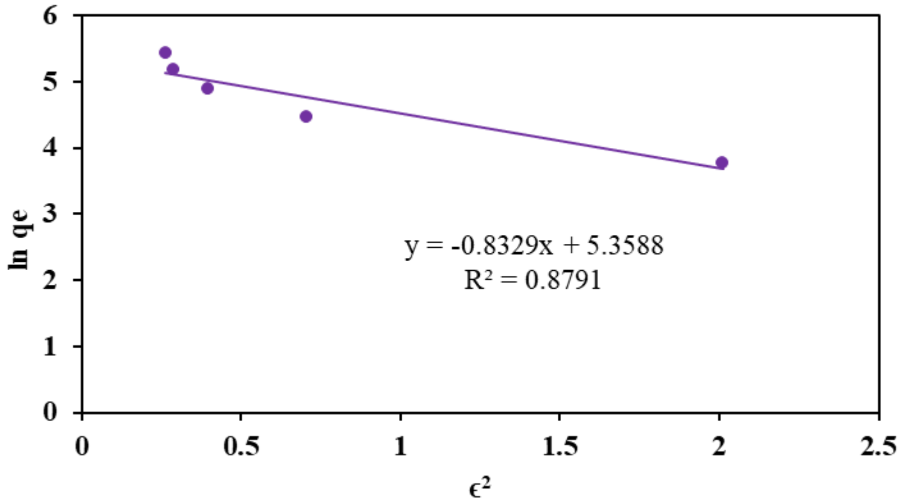

(iv)

Fig. 9. Isotherms (i) Langmuir (ii) Freundlich (iii) Temkin (iv) D-R

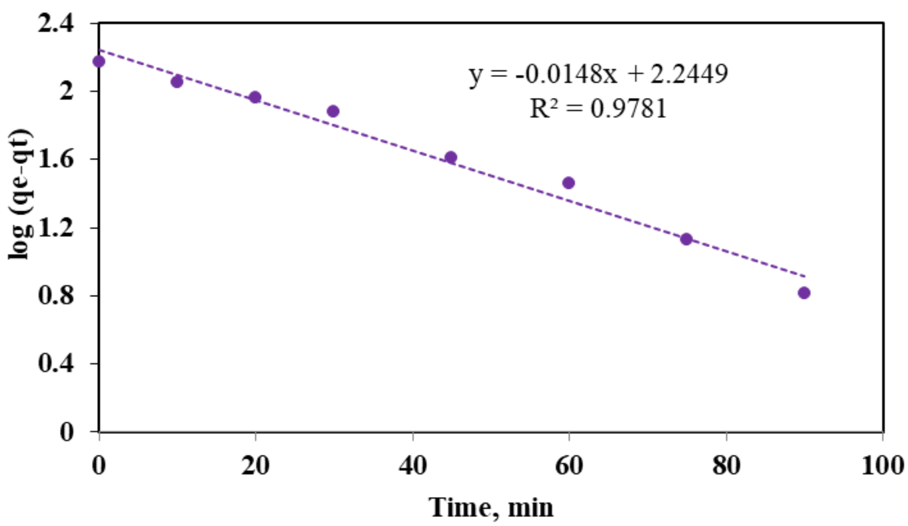

(i)

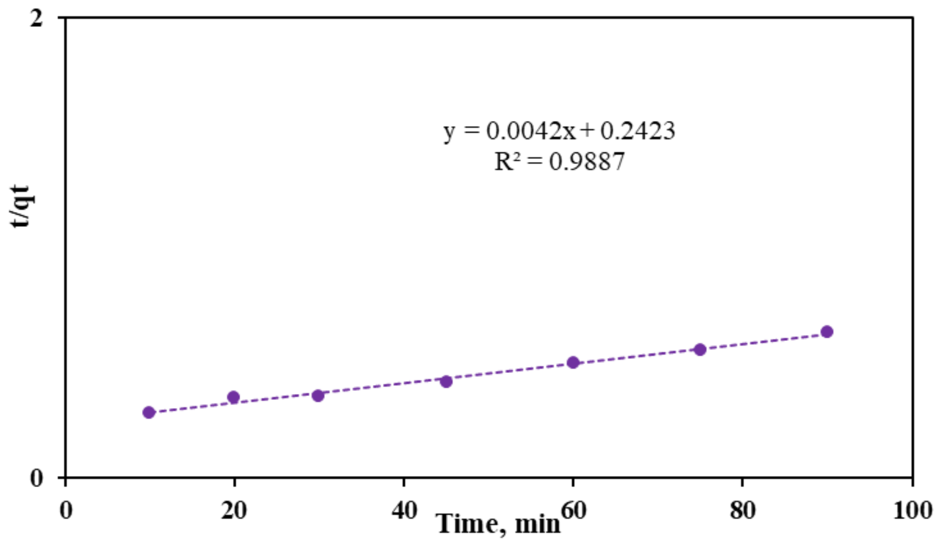
2
0
t/qt
y = 0.0042x + 0.2423
R² = 0.9887
0
20
40
60
80
100
Time, min

(ii)

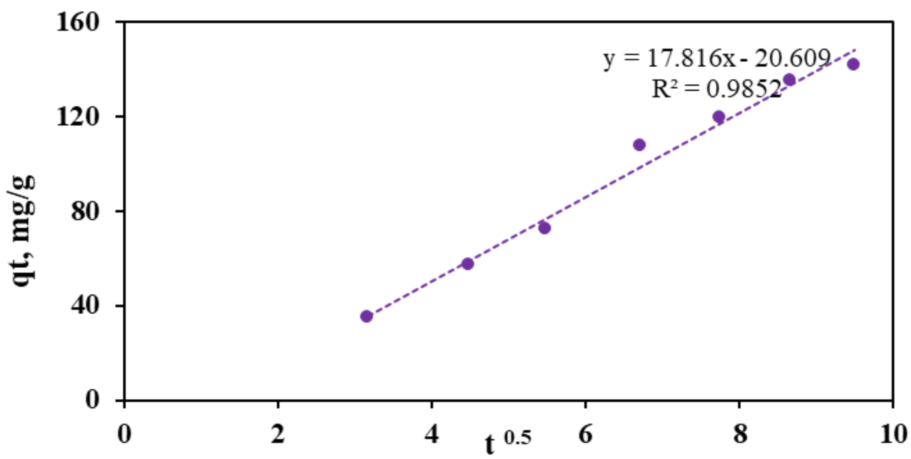
160
120
80
40
0
qt, mg/g
y = 17.816x - 20.609
R² = 0.9852
0
2
4
6
8
10
t 0.5

(iii)

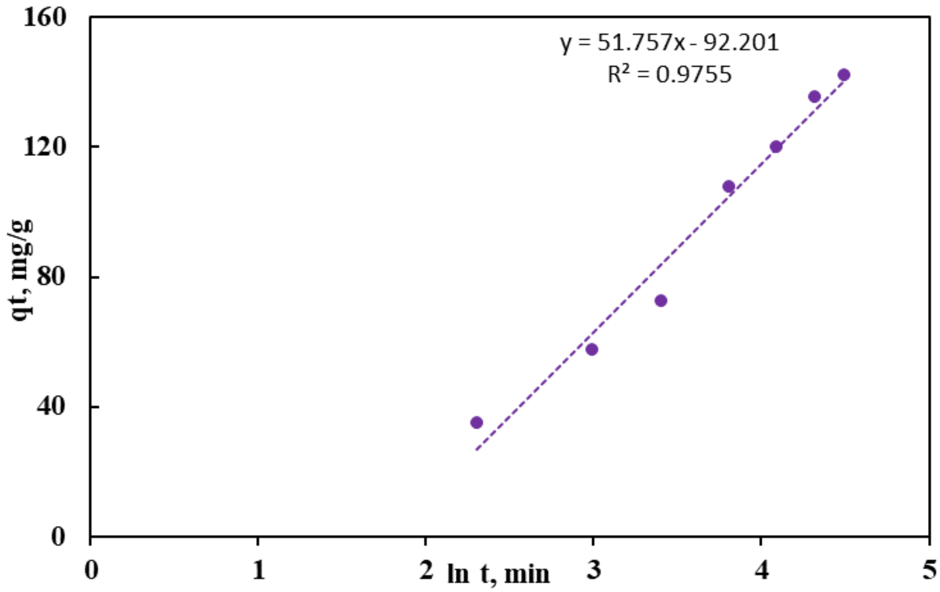

(iv)

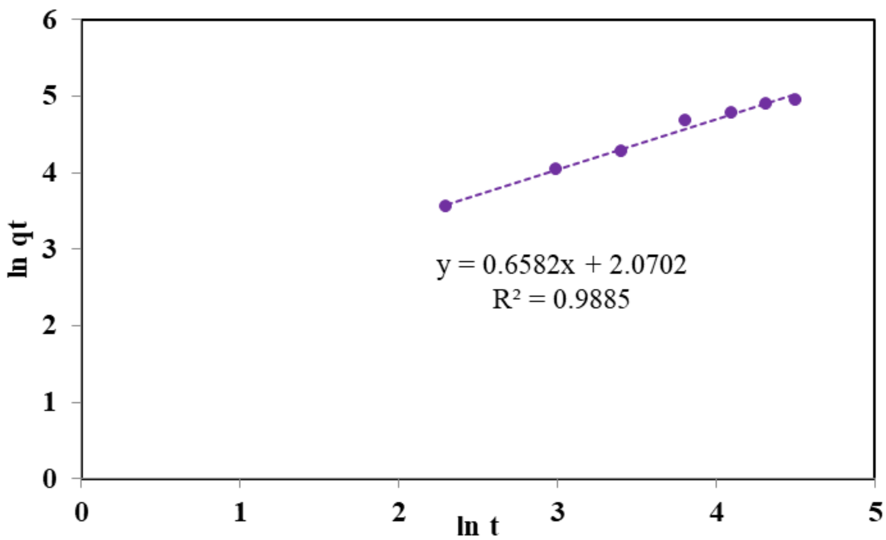

(v)

Fig.10. Kinetics (i) PFO (ii) PSO (iii) IPD (iv) Elovich (v) Power model

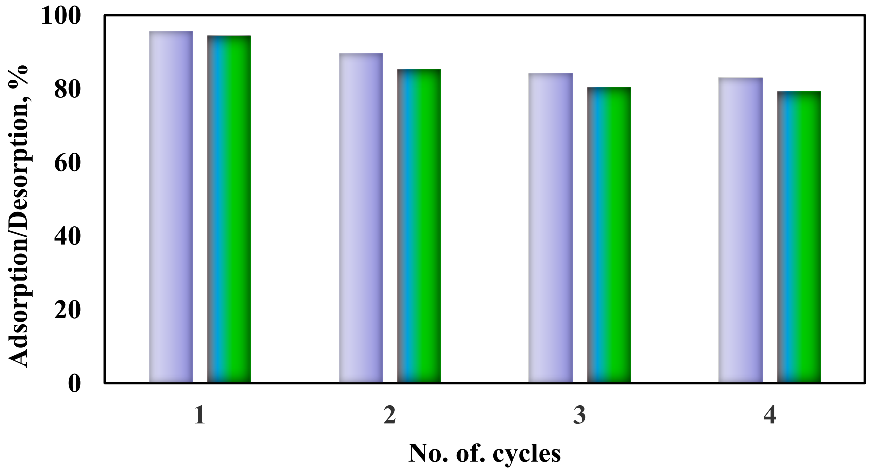

Fig. 11. Reusability of biochar composite in different cycles

Table 1 Parameter ranges for sorptive removal of congo red

Variables	Code	Levels		
		-1	0	1
pH	A	2	7	12
CR IC (mg/L)	B	10	50	90
AS (rpm)	C	100	300	500

Table 2 BBD for CR removal using Polyaniline modified Fe_3O_4 loaded Delonix regia seed biochar nanocomposite

Std order	pH	CR IC (mg/L)	AS (rpm)	% Removal of CR	
				Experimental	Predicted
1	2	10	300	39.61	39.05
2	12	10	300	53.25	52.15
3	2	90	300	53.81	53.51
4	12	90	300	63.06	63.16
5	2	50	100	34.00	33.90
6	12	50	100	44.36	44.86
7	2	50	500	86.50	85.20
8	12	50	500	99.05	99.25
9	7	10	100	25.68	25.58
10	7	90	100	44.48	44.18
11	7	10	500	86.08	85.08
12	7	90	500	91.28	91.58
13	7	50	300	91.63	90.83
14	7	50	300	91.63	92.23
15	7	50	300	91.63	91.21
16	7	50	300	91.63	91.03
17	7	50	300	91.63	90.13

Table 3 ANOVA for CR removal using Polyaniline modified Fe_3O_4 loaded Delonix regia seed biochar nanocomposite

Source	Sum of Squares	df	Mean Square	F-value	P-value
Model	10243.46	9	1138.16	1.06 E+08	< 0.0001
A-pH	262.20	1	262.20		< 0.0001
B-Concentration	288.12	1	288.12	29522827	< 0.0001
C-RPM	5745.38	1	5745.38	3.14E+08	< 0.0001
AB	4.82	1	4.82	449682.3	< 0.0001
AC	1.20	1	1.20	111909	< 0.0001
BC	46.24	1	46.24	4315733	< 0.0001
A^2	1296.85	1	1296.85	1.21E+08	< 0.0001
B^2	1973.11	1	1973.11	1.84E+08	< 0.0001
C^2	276.42	1	276.42	25799497	< 0.0001
Residual	0.0001	7	0.0000		
Lack of Fit	0.0001	3	0.0000		
Pure Error	0.0000	4	0.0000		
Cor Total	10243.46	16			

R^2 -0.9995; Adj R^2- 0.9872;Pred R^2 - 0.2750; PRESS-5874.68; Adeq Precision- 76.98

Table 4 Thermodynamic study results

Temp(K)	ΔG° (kJ/mol)	ΔS° (kJ/mol k)	ΔH° (kJ/mol)
298	-8.64509		
303	-8.92662		
308	-9.2837	0.0717	12.715
313	-9.75349		
318	-10.4208		
323	-10.415		
328	-10.6192		

Table 5 Isotherm study results for CR sorption

Isotherm	Model	Reference	Parameters	Values
Langmuir	$\frac{1}{q_e} = \frac{1}{q_m b C_e} + \frac{1}{q_m}$	Langmuir et al. (1918)	q_m (mg/g)	384.615
			b (L/mg)	0.076
			R^2	0.9954
Freundlich	$\log_{10} q_e = \log_{10} K_f + \frac{1}{n} \log_{10} C_e$	Freundlich et al. (196)	K_f (L/mg)	28.464
			1/n	1.2975
			R^2	0.9749
Dubinin-Redushkevich	$\ln q_e = \ln q_m - \beta \varepsilon^2$	Dubinin et al. (1960)	q_m (mg/g)	212.46
			β (mol^2/kJ$^{2)}$	0.8329
			E (kJ/mol)	0.7747
			R^2	0.8791
Temkin	$q_e = B \ln K_T + B \ln C_e$	Temkin et al. (1940)	B	310.97
			K_T (L/mg)	0.9630
			R^2	0.8506

Table 6 Kinetic models used for CR sorption

Kinetics	Model	Reference	Parameters	Values
Pseudo first order	$\ln(q_e - q_t) = \ln(q_e) - k_1 t$	Ho and Yuh-Shan (2004)	K_1(min^{-1})	0.00642
			R^2	0.9781
			qe, cal (mg/g)	9.4394
Pseudo second order	$\frac{t}{q_t} = \frac{1}{k_2 q_e^2} + \frac{t}{q_e}$	Ho and McKay (1999)	K_2((g/mg)min)	$4.27x10^{-6}$
			R^2	0.9887
			qe, cal (mg/g)	238.095
Intra particle diffusion	$q_t = k_{id} t^{0.5} + C$	Weber and Morris (1963)	K_{id}((mg/g)$min^{-0.5}$)	17.816
			C	-20.919
			R^2	0.9852
Elovich	$q_t = \frac{1}{\beta}\ln(\alpha\beta) + \frac{1}{\beta}\ln t$	Juang and Chen (1997)	α	307.487
			β	0.0193
			R^2	0.9755
Power function	$\log q_t = \log k + v \log t$	Pandian et al. (2017)	k	2.0702
			v	0.6582
			R^2	0.9885

Table 7 Sorption ability of different sorbents for CR removal

Composites	Sorption capacity, mg/g	References
Biochar from green pea waste	62.11	Norbert Onen *et al*. (2023)
ZnO modified hybrid biochar from green pea waste	114.94	Norbert Onen *et al*. (2023)
Magnetic self-nitrogen-doped biochar	1360	Xinyu *et al*. (2023)

Algal biochar-based nanocomposite	34.53	
Nitrogen self-doped biochar from soybean cake	882.64	Xinyu *et al*. (2022)
ZIF-8 biochar from recycled coffee grounds	1080.4	Yixuan *et al*. (2022)
Algal biochar-based nanocomposite	34.53	Wasim *et al*. (2021)
Porous biochar obtained from pistachio shells	614.7	Summaira *et al*. (2022)
Nano-zerovalent manganese/biochar composite	117.647	Jibran *et al*. (2021)
Wet-torrefied Chlorella sp. microalgal biochar	164.35	Kai Ling *et al*. (2021)
Silver nanoparticle doped mesoporous biochar	23.39	Wasim *et al*. (2022)
Polyethyleneimine modified $CoFe_2O_4$-loaded porous biochar	435.9	Zhengde *et al*. (2021)
Copper doped walnut shell-based biochar	248.2	Qizhao *et al*. (2021)
Litchi peel biochar	404.4	Jia *et al*. (2020)
Calcium-rich biochar from crab shell	20317	Lichun *et al*. (2018)
Polyaniline modified Fe_3O_4 loaded Delonix regia seed biochar	384.615	Present study

References

Agilandeswari, P., Venkateshbabu, S., Sarojini, G. & Rajasimman, M. (2024a) Sustainable development and analysis of a novel bio-derived (biochar) nanocomposite for the remediation of carbamazepine from aqueous solution, *Chemosphere*, 347, 140696. https://doi.org/10.1016/j.chemosphere.

Agilandeswari, P., Venkateshbabu, S., Sarojini, G., Rajamohan, N. & Rajasimman, M. (2024b) Valorization of biowaste for nanocomposite synthesis and its application for the environmental remediation of bisphenol A: Optimization, model evaluation and docking studies, *Waste and Biomass Valorization*. https://doi.org/10.1007/s12649-023-02316-z.

Ahmad, M.A., Ahmad, N. & Bello, O.S. (2015) Modified durian seed as adsorbent for the removal of methyl red dye from aqueous solutions, *Applied Water Science*, 5, 407–423.

Ambaye, T.G., Mentore, V., Prasad, S., Eric, D., van, H. & Rtimi, S. (2022) Preparation and applications of chitosan and cellulose composite materials, *Journal of Environmental Management*, 301, 113850. https://doi.org/10.1016/j.jenvman.2021.113850.

Amen, R., Yaseen, M., Mukhtar, A., Klemeš, J.J., Saqib, S., Ullah, S., Al-Sehemi, A.G., Rafiq, S., Babar, M., Lai Fatt, C., Ibrahim, M., Asif, S., Qureshi, K.S., Akbar, M.M. & Bokhari, A. (2020) Lead and cadmium removal from wastewater using eco-friendly biochar adsorbent derived from rice husk, wheat straw, and corncob, *Cleaner Engineering and Technology*, 1, 100006. https://doi.org/10.1016/j.clet.2020.100006.

Awang, M., Zuki, A.A.A., Mahmud, A.A., Jaafar, J.J. & Zain, M.H. (2017) Application of microwave-treated *Casuarina equisetifolia* seeds in adsorption of dyes, *Journal of Fundamental and Applied Sciences*, 9(7S), 458–471. https://doi.org/10.4314/jfas.v9i7s.43.

Chen, X., Di, Z., Huaiyin, C. & Ruoyu, H. (2021) Preparation and characterization of CIP@Fe_3O_4@PANI composites, *Colloids and Surfaces A: Physicochemical and Engineering Aspects*, 628, 127410. https://doi.org/10.1016/j.colsurfa.2021.127410.

Dai, L.C., Zhu, W.K., He, L., Tan, F.R., Zhu, N.M., Zhou, Q., He, M.X. & Hu, G.Q. (2018) Calcium-rich biochar from crab shell: an unexpected super adsorbent for dye removal, *Bioresource Technology*, 267, 510–516.

Dubinin, M. (1960) The potential theory of adsorption of gases and vapors for adsorbents with energetically nonuniform surfaces, *Chemical Reviews*, 60, 235–241.

Emenike, E.C., Samuel, O., Joshua, O.I., Iwuozor, K.O., Okoro, H.K. & Adeniyi, A.G. (2022 *Delonix regia* biochar potential in removing phenol from industrial wastewater, *Bioresource Technology Reports*, 19, 101195. https://doi.org/10.1016/j.biteb.2022.101195

Freundlich, H. (1906) Over the adsorption in solution, *Journal of Physical Chemistry*, 57, 1100–1107.

Ho, Y.S. & McKay, G. (1999) Pseudo-second order model for sorption processes, *Process Biochemistry*, 34, 451–465. https://doi.org/10.1016/S0032-9592(98)00112-5.

Ho, Y.S. (2004) Citation review of Lagergren kinetic rate equation on adsorption reactions, *Scientometrics*, 59, 171–177.

Hossain, N., Nizamuddin, S., Selvakannan, P., Griffin, G., Madapusi, S. & Shah, K. (2022) The effect of KOH activation and Ag nanoparticle incorporation on rice husk-based porous materials for wastewater treatment, *Chemosphere*, 291(3), 132760. https://doi.org/10.1016/j.chemosphere.2021.132760.

Islam, M.N., Khan, A.K., Mallik, M.M. & Rahman, M. (2019) Preparation of bio-inspired trimethoxysilyl group terminated poly(1-vinylimidazole)-modified-chitosan composite for a adsorption of chromium (VI) ions, Journal of Hazardous Materials, 379, 120792. https://doi.org/10.1016/j.jhazmat.2019.120792.

Jayakumar, V., Govindaradjane, S., Rajamohan, N. & Rajasimman, M. (2021) Sustainable removal of cadmium from contaminated water using green alga – Optimization, characterization and modeling studies, *Environmental Research*, 199, 111364. =https://doi.org/10.1016/j.envres.2021.111364.

Jia, W., Jianwei, Y., Pu, F., Huang, G., Xu, C. & Lin, B. (2020) High-efficiency removal of dyes from wastewater by fully recycling litchi peel biochar, *Chemosphere*, 246, 125734. https://doi.org/10.1016/j.chemosphere.2019.125734

Jiang, T., Wang, B., Gao, B., Cheng, N., Feng, Q., Chen, M. & Wang, S. (2023) Degradation of organic pollutants from water by biochar-assisted advanced oxidation processes: Mechanisms and applications, *Journal of Hazardous Materials*, 442, 130075. https://doi.org/10.1016/j.jhazmat.2022.130075.

Jibran, I., Shah, N.S., Sayed, M., Niazi, N.K., Imran, M., Khan, J.A., Khan, Z.U.H., Hussien, A.G.S., Polychronopoulou, K. & Howari, F. (2021) Nano-zerovalent manganese/biochar composite for the adsorptive and oxidative removal of Congo-red dye from aqueous solutions, *Journal of Hazardous Materials*, 403, 123854. https://doi.org/10.1016/j.jhazmat.2020.123854.

Juang, R.S. & Chen, M.L. (1997) Application of the Elovich equation to the kinetics of metal sorption with solvent-impregnated resins, *Industrial & Engineering Chemistry Research*, 36, 813–820.

Kataria, N. & Garg, V.K. (2018) Green synthesis of Fe_3O_4 nanoparticles loaded sawdust carbon for cadmium (II) removal from water: Regeneration and mechanism, *Chemosphere*, 208, 818–828. https://doi.org/10.1016/j.chemosphere.2018.06.022.

Kumar, R., Bhattacharya, S. & Sharma, P. (2021) Novel insights into adsorption of heavy metal ions using magnetic graphene composites, *Journal of Environmental Chemical Engineering*, 9(5), 106212. https://doi.org/10.1016/j.jece.2021.106212.

Langmuir, I. (1918) The adsorption of gases on plane surfaces of glass, mica and platinum, *Journal of the American Chemical Society*, 40, 1361–1403

Lee, X.J., Lee, L.Y., Gan, S., Thangalazhy-Gopakumar, S. & Ng, H.K. (2017) Biochar potential evaluation of palm oil wastes through slow pyrolysis: Thermochemical characterization and pyrolytic kinetic studies, *Bioresource Technology*, 236, 155–163. https://doi.org/10.1016/j.biortech.2017.03.105.

Li, Y., Ju, W., Yang, L., Zhang, L. & Sun, Y. (2020) Adsorption behaviors and mechanism of graphene oxide for silver complex anion removal, Applied Surface Science, 529, 147112. https://doi.org/10.1016/j.apsusc.2020.147112.

Li, Y., Li, H., Li, X., Zhang, Q., Fei, J., Li, S. & Chen, S. (2022) Using recycled coffee grounds for the synthesis of ZIF-8@BC to remove Congo red in water, *Ecotoxicology and Environmental Safety*, 236, 113450. https://doi.org/10.1016/j.ecoenv.2022.113450.

Lian, G., Wang, B., Lee, X., Li, L., Liu, T. & Lyu, W. (2019) Enhanced removal of hexavalent chromium by engineered biochar composite fabricated from phosphogypsum and distillers grains, Science of The Total Environment, 697, 134119. https://doi.org/10.1016/j.scitotenv.2019.134119.

Lichun, D., Zhu, W., Li, H., Furong, T., Zhu, N., Zhou, Q., He, M. & Hu, G. (2018) Calcium-rich biochar from crab shell: An unexpected super adsorbent for dye removal, *Bioresource Technology*, 267, 510–516. https://doi.org/10.1016/j.biortech.2018.07.090.

Ling, Y.K., Lee, X.J., Ong, H.C., Chen, W.H., Lin, C.S., Loke, S.P. & Chuan, L.T. (2021) Adsorptive removal of cationic methylene blue and anionic Congo red dyes using wet-torrefied microalgal biochar: Equilibrium, kinetic and mechanism modeling, *Environmental Pollution*, 272, 115986. https://doi.org/10.1016/j.envpol.2020.115986.

Mao, W., Zhang, Y., Luo, J., Chen, L. & Guan, Y. (2022) Novel co-polymerization of polypyrrole/polyaniline on ferrate modified biochar composites for the efficient adsorption of hexavalent chromium in water, *Chemosphere*, 303(3), 135254. https://doi.org/10.1016/j.chemosphere.2022.135254.

Mondal, P., Anweshan, A. & Purkait, M. (2020) Green synthesis and environmental application of iron-based nanomaterials and nanocomposite: A review, *Chemosphere*, 259, 127509. https://doi.org/10.1016/j.chemosphere.2020.127509.

Onen, R.N., Elkady, M., Ahmed, E., Fujita, M., Sekiguchi, H. & Shokry, H.S. (2023) Effective decontamination of methylene blue from aqueous solutions using novel nano-magnetic biochar from green pea peels, *Environmental Research*, 220, 115272. https://doi.org/10.1016/j.envres.2023.115272.

Pandian, A.M.K., Karthikeyan, C. & Rajasimman, M. (2017) Isotherm and kinetic studies on adsorption of malachite green using chemically synthesized silver nanoparticles, *Nanotechnology for Environmental Engineering*, 2(2). https://doi.org/10.1007/s41204-016-0013-4.

Park, M.H., Jeong, S. & Kim, J.Y. (2019) Adsorption of NH_3-N onto rice straw-derived biochar, *Journal of Environmental Chemical Engineering*, 7(2), 103039. https://doi.org/10.1016/j.jece.2019.103039.

Rai, M.K., Giri, B.S., Nath, Y., Bajaj, S., Soni, S., Singh, R.P., Singh, R.S. & Rai, B.N. (2018) Adsorption of hexavalent chromium from aqueous solution by activated carbon prepared from almond shell: kinetics, equilibrium and thermodynamics study, *Journal of Water Supply: Research and Technology - Aqua*, 67(8), 724–737.

Reghioua, A., Barkat, D., Ali, H.J., Abdulhameed, A.S. & Khan, M.R. (2021) Synthesis of Schiff's base magnetic crosslinked chitosan-glyoxal/ZnO/Fe_3O_4 nanoparticles for enhanced adsorption of organic dye: Modeling and mechanism study, *Sustainable Chemistry and Pharmacy*, 20, 100379. https://doi.org/10.1016/j.scp.2021.100379.

Sarojini, G., Kannan, P., Rajmohan, N. & Rajasimman, M. (2023) Bio-fabrication of porous magnetic Chitosan/Fe_3O_4 nanocomposite using Azolla pinnata for removal of Chromium – parametric effects, surface characterization and kinetics, Environmental Research, 218, 114822. https://doi.org/10.1016/j.envres.2022.114822.

Sarojini, G., Venkatesh Babu, S., Rajamohan, N., Senthil Kumar, P. & Rajasimman, M. (2021) Surface modified polymer-magnetic-algae nanocomposite for the removal of chromium—equilibrium and mechanism studies, *Environmental Research*, 201, 111626. https://doi.org/10.1016/j.envres.2021.111626.

Sarojini, G., Venkateshbabu, S. & Rajasimman, M. (2022) Adsorptive potential of iron oxide based nanocomposite for the sequestration of Congo red from aqueous solution, *Chemosphere*, 287, 132371. https://doi.org/10.1016/j.chemosphere.2021.132371.

Shaheen, J., Yohanna Haile, F. & Sizirici, B. (2022) Performance, life cycle assessment, and economic comparison between date palm waste biochar and activated carbon derived from woody biomass, Heliyon, 8(12), e12388. https://doi.org/10.1016/j.heliyon.2022.e12388.

Shaikh, W.A., Chakraborty, S., Ul Islam, R., Ghfar, A.A., Naushad, M., Bundschuh, J., Maity, J.P. & Mondal, N.K. (2022) Fabrication of biochar-based hybrid Ag nanocomposite from algal biomass waste for toxic dye-laden wastewater treatment, *Chemosphere*, 289, 133243. https://doi.org/10.1016/j.chemosphere.2021.133243.

Shakoor, M.B., Khan, N.N., Bibi, I., Shahid, M., Saqib, Z.A., Nawaz, M.F., Shaheen, S.M., Wang, H., Daniel, C.W., Tsang, Y.S.O., Bundschuh, J. & Jörg, R. (2019) Exploring the arsenic removal potential of various biosorbents from water, Environment International, 123, 567–579. https://doi.org/10.1016/j.envint.2018.12.049.

Sharma, V., Singh, H., Guleria, S., Bhardwaj, N., Puri, S., Arya, S.K. & Khatri, M. (2022) Application of superparamagnetic iron oxide nanoparticles (SPIONs) for heavy metal adsorption: A 10-year meta-analysis, *Environmental Nanotechnology, Monitoring & Management*, 18, 100716. https://doi.org/10.1016/j.enmm.2022.100716.

Sonwani, R.K., Swain, G., Giri, B.S., Singh, R.S. & Rai, B.N. (2020) Biodegradation of Congo red dye in a moving bed biofilm reactor: Performance evaluation and kinetic modeling, *Bioresource Technology*, 302, 122811. https://doi.org/10.1016/j.biortech.2020.122811.

Summaira, S., Pu, C., Fu, E., Wang, Y. & Xiao, Z. (2022) Synthesis of high surface area porous biochar obtained from pistachio shells for the efficient adsorption of organic dyes from polluted water, *Surface Interfaces*, 34, 102357. https://doi.org/10.1016/j.surfin.2022.102357.

Sun, H., Hockaday, W.C., Mastello, C.A. & Zygourakis, K. (2012) Multiple controls on the chemical and physical structure of biochars, *Industrial & Engineering Chemistry Research*, 51, 3587–3597.

Sun, Q., Li, Y., Wang, Q., Niu, T., Li, S. & Shen, W. (2021) Preparation of copper doped walnut shell-based biochar for efficient removal of organic dyes from aqueous solutions, *Journal of Molecular Liquids*, 336, 116314. https://doi.org/10.1016/j.molliq.2021.116314.

Talha, M., Goswami, M., Giri, B.S., Sharma, A., Rai, B.N. & Singh, R.S. (2018) Bioremediation of Congo red dye in immobilized batch and continuous packed bed bioreactor by Brevibacillus parabrevis using coconut shell bio-char, Bioresource Technology, 252, 37–43. https://doi.org/10.1016/j.biortech.2017.12.081.

Tan, C., Zhou, Z., Xu, S., Wang, H. & Lu, W. (2015) Adsorption behavior comparison of trivalent and hexavalent chromium on biochar derived from municipal sludge, *Bioresource Technology*, 190, 388–394. https://doi.org/10.1016/j.biortech.2015.04.115.

Tang, J., Lv, H., Gong, Y. & Huang, Y. (2015) Preparation and characterization of a novel graphene/biochar composite for aqueous phenanthrene and mercury removal, Bioresource Technology, 196, 355–363. https://doi.org/10.1016/j.biortech.2015.07.047.

Temkin, M. (1940) Kinetics of ammonia synthesis on promoted iron catalysts, *Acta Physicochimica URSS*, 12, 327–356.

Thomas, D., Noeline, B., Fernandez, C., Mullassery, M.D. & Surya, R. (2020) Iron oxide loaded biochar/polyaniline nanocomposite: Synthesis, characterization and electrochemical analysis, *Inorganic Chemistry Communications*, 119, 108097. https://doi.org/10.1016/j.inoche.2020.108097.

Tran, V.S., Ngo, H.H., Guo, W., Zhang, J., Liang, S., Ton-That, C. & Zhang, X. (2015) Typical low-cost biosorbents for adsorptive removal of specific organic pollutants from water, Bioresource Technology, 182, 353–363. https://doi.org/10.1016/j.biortech.2015.02.003.

Vikrant, K., Shekhar, G.B., Raza, N., Roy, K., Ki-Hyun, K., Rai, B.N. & Singh, R.S. (2018) Recent advancements in bioremediation of dye: Current status and challenges, *Bioresource Technology*, 253, 355–367. https://doi.org/10.1016/j.biortech.2018.01.029.

Wang, Z., Wang, X., Yao, J., Zhan, S., Li, H., Zhang, J. & Qiu, Z. (2021) Synthesis of polyethyleneimine modified $CoFe_2O_4$-loaded porous biochar for selective adsorption properties towards dyes and exploration of interaction mechanisms, *Separation and Purification Technology*, 277, 119474. https://doi.org/10.1016/j.seppur.2021.119474.

Wasim, A.S., Chakraborty, S., Ul Islam, R., Ghfar, A.A., Naushad, M., Bundschuh, J., Maity, J.P. & Mondal, N.K. (2022) Fabrication of biochar-based hybrid Ag nanocomposite from algal biomass waste for toxic dye-laden wastewater treatment, *Chemosphere*, 289, 133243. https://doi.org/10.1016/j.chemosphere.2021.133243.

Wasim, A.S., Ul Islam, R. & Chakraborty, S. (2021) Stable silver nanoparticle doped mesoporous biochar-based nanocomposite for efficient removal of toxic dyes, *Journal of Environmental Chemical Engineering*, 9(1), 104982. https://doi.org/10.1016/j.jece.2020.104982.

Weber, W.J. & Morris, J.C. (1963) Kinetics of adsorption on carbon from solution, *Journal of the Sanitary Engineering Division*, 89, 31–60.

Yu, C., Tang, J., Su, H., Huang, J., Liu, F., Wang, L. & Sun, H. (2022) Development of a novel biochar/iron oxide composite from green algae for bisphenol-A removal: Adsorption and Fenton-like reaction, *Environmental Technology & Innovation*, 28, 102647. https://doi.org/10.1016/j.eti.2022.102647.

Zhang, K., Huang, K., Liang, Y., Hu, H., Xu, X., Chen, D. & Wang, Y. (2023) Dense and uniform growth of TiO_2 nanoparticles on the pomelo-peel-derived biochar surface for efficient photocatalytic antibiotic degradation, Journal of Environmental Chemical Engineering, 11(2), 109358. https://doi.org/10.1016/j.jece.2023.109358.

Zhang, X., Liu, M. & Han, R. (2021) Adsorption of phosphate on UiO-66-NH_2 prepared by green synthesis method, *Journal of Environmental Chemical Engineering*, 9(6), 106672. https://doi.org/10.1016/j.jece.2021.106672.

Zhang, X., Nguyen, T.H., Liu, Y., Yang, C., Zhang, T., Guo, J., Zhu, W., Ahmad, M., Xiao, H. & Song, J. (2023) Nitrogen-doped magnetic biochar made with $K_3[Fe(C_2O_4)_3]$ to adsorb dyes: Experimental approach and density functional theory modeling, *Journal of Cleaner Production*, 383, 135527. https://doi.org/10.1016/j.jclepro.2022.135527.

Zhang, X., Tian, J., Wang, P., Liu, T., Ahmad, M., Zhang, T., Guo, J., Xiao, H. & Song, J. (2022) Highly-efficient nitrogen self-doped biochar for versatile dyes' removal prepared from soybean cake via a simple dual-templating approach and associated thermodynamics, *Journal of Cleaner Production*, 332, 130069. https://doi.org/10.1016/j.jclepro.2021.130069.

Zhang, Y., Xu, X., Cao, L., Ok, Y.S. & Cao, X. (2018) Characterization and quantification of electron donating capacity and its structure dependence in biochar derived from three waste biomasses, Chemosphere, 211, 1073–1081. https://doi.org/10.1016/j.chemosphere.2018.08.033.

Zheng, H., Qi, J., Jiang, R., Gao, Y. & Li, X. (2015) Adsorption of malachite green by magnetic litchi pericarps: A response surface methodology investigation, *Journal of Environmental Management*, 162, 232–239. https://doi.org/10.1016/j.jenvman.2015.07.057.

Zhou, Q., Wang, Y., Xiao, J. & Fan, H. (2016) Adsorption and removal of bisphenol A, α-naphthol and β-naphthol from aqueous solution by Fe_3O_4@polyaniline core shell nanomaterials, *Synthetic Metals*, 212, 113–122.

Zhou, Q., Wang, Y., Xiao, J. & Zhan, Y. (2019) Preparation of magnetic core-shell Fe_3O_4@polyaniline composite material and its application in adsorption and removal of tetrabromobisphenol A and decabromodiphenyl ether, *Ecotoxicology and Environmental Safety*, 183, 109471. https://doi.org/10.1016/j.ecoenv.2019.109471.

Zhu, H., Li, L., Chen, W., Tong, Y. & Wang, X. (2021) Controllable synthesis of coral-like hierarchical porous magnesium hydroxide with various surface area and pore volume for lead and cadmium ion adsorption, Journal of Hazardous Materials, 416, 125922. https://doi.org/10.1016/j.jhazmat.2021.125922.